PCCP

Mapping spin contamination-free potential energy surfaces using restricted open-shell methods with Grassmannians

Journal:	*Physical Chemistry Chemical Physics*
Manuscript ID	CP-ART-11-2023-005437.R1
Article Type:	Paper
Date Submitted by the Author:	11-Dec-2023
Complete List of Authors:	Tan, Jake; University of Richmond, Chemistry Lao, Ka Un; Virginia Commonwealth University, Chemistry

Journal Name

ARTICLE TYPE

Cite this: DOI: 00.0000/xxxxxxxxxx

Mapping spin contamination-free potential energy surfaces using restricted open-shell methods with Grassmannians†

Jake A. Tan*[a] and Ka Un Lao*[b]

Received Date
Accepted Date

DOI: 00.0000/xxxxxxxxxx

The Lagrange-based Grassmann interpolation (G-Int) method has been extended for open-shell systems using restricted open-shell (RO) methods. The performance of this method was assessed in constructing potential energy surfaces (PESs) for vanadiun (II) oxide, benzyl radical, and methanesulfenyl chloride radical cation. The density matrices generated by G-Int when used as initial guesses for self-consistent field (SCF) calculations, exhibit superior performance compared to other traditional SCF initial guess schemes, such as SADMO, GWH, and CORE. Additionally, the energy obtained from the G-Int scheme satisfies the variational principle and outperforms the direct energy-based Lagrange interpolation approach. In the case of methanesulfenyl chloride radical cation, a unique example with a flat PES at the end region along the H-C-S-Cl dihedral angle, the use of an equally-spaced grid sampling leads to significant oscillations near the end of the interval due to the effects of Runge's phenomenon. Introducing an unequally-spaced grid sampling based on a scaled Gauss-Chebyshev quadrature effectively mitigated the Runge's phenomenon, making it suitable for combining with G-Int in constructing PESs for general applications. Thus, G-Int provides an efficient and robust strategy for building spin contamination-free PESs with consistent accuracy.

1 Introduction

Modeling electronic structure of open-shell species is essential to obtain their properties relevant to spectroscopy and excited-state processes.[1] The unrestricted (U) variant[2] of Hartree-Fock (HF), density functional theory (DFT), and post-HF through the use of a single Slater determinant with two sets of optimized orbitals (α and β) is always the first choice to describe open-shell systems.[1] However, the unrestricted variant suffers from spin contamination which is a long standing problem owing to the incorporation of higher spin state character.[2] Spin contamination may become a difficult issue in transition metal complexes, radical chemistry, and bond dissociation, such as predictions of geometries, electronic state ordering, as well as vibrational modes, the shape of the potential energy surface (PES), vertical detachment energies, and discrepancies between theoretical and experimental spectra.[3–5] An alternative to the unrestricted variant is the restricted open-shell (RO) variant, where molecular orbitals are constrained to be doubly occupied as much as possible in open-shell systems. An advantage of the restricted open-shell over the unrestricted variant is that the wavefunction is an eigenstate of the total spin operator $\hat{\mathbf{S}}^2$ and therefore RO computational results are spin contamination free. Nevertheless, restricted open-shell methods fail to describe spin polarization, tend to converge slower than their unrestricted counterparts, and are less commonly available in quantum chemistry software. As a result, even suffering from spin contamination, much of the open-shell systems are studied using the unrestricted variant, especially in mapping PESs which need many *ab initio* calculations. One can ameliorate some of the problems caused by spin contamination in unrestricted calculations using spin projection techniques.[3] However, spin projection may create unphysical cusps (*i.e.,* derivative discontinuities) on potential energy curves.[6] Thus, restricted open-shell variant is still the preferred method to generate spin contamination-free PESs if its slow convergence issue can be overcome. This work will introduce a method to generate a good self-consistent field (SCF) initial guess in solving the Roothaan-Hall equation[2] for restricted open-shell methods which can reduce the number of RO-SCF cycles to accelerate convergence.

An initial guess density matrix $\mathbf{P}_{\text{guess}}$ is used to build the Fock matrix $\mathbf{F}$ for starting the SCF iteration procedure. Traditionally, this guess can come from well-established schemes such as the superposition of atomic densities (SAD),[7] purified SAD (SADMO),[8] core Hamiltonian (CORE), and generalized Wolfsberg−Helmholtz (GWH).[9] Afterward, $\mathbf{F}$ is used to solve for the Roothaan-Hall equation ($\mathbf{FC} = \mathbf{SCE}$) to obtain the molecular orbital (MO) coefficient matrix $\mathbf{C}$ and the MO energy matrix $\mathbf{E}$, where $\mathbf{S}$ is the overlap matrix. From the occupied MOs in $\mathbf{C}$,

[a] Department of Chemistry, Gottwald Center for the Sciences, University of Richmond, Richmond, VA , USA. E-mail: jake.tan@richmond.edu
[b] Department of Chemistry, Virginia Commonwealth University, Richmond, VA, USA. E-mail: laoku@vcu.edu

† Electronic supplementary information (ESI) available: Additional calculations and analysis. See DOI: 00.0000/00000000.

a new density matrix is built via $\mathbf{P} = \mathbf{C}^{\text{occ}}(\mathbf{C}^{\text{occ}})^{\mathbf{T}}$. A new Fock matrix is then built again, and the previous steps are repeated until self-consistency is achieved with respect to a certain convergence criteria. It is known that the number of SCF cycles needed to reach convergence depends on the quality of the initial guess, $\mathbf{P}_{\text{guess}}$.[10] A good initial guess will require fewer SCF cycles, while a poor initial guess will require more SCF cycles or even worse lead to SCF convergence issues.[10–13]

Exploring a potential energy surface (PES) is a commonly performed computational study in chemical research, where one has to do many SCF calculations along different molecular geometries for mapping out the surface. One of the current practice is to use a sparse grid obtained from *ab initio* calculations to build a PES. Afterward, an energy-based (EB) interpolation scheme[14] is performed to refine the PES. Instead of performing direct EB interpolations, density matrix (DM)-based interpolations, which have been realized recently ,[11,12,15] can also be performed. The development of DM-based interpolations has been hampered, because density matrices do not obey closure property where a linear combination of density matrices does not necessarily yield another density matrix.[11] In other words, the interpolated density matrix $\mathbf{P}_{\text{interp}}$ does not necessarily satisfy three physical requirements including (1) $\mathbf{P}_{\text{interp}} = \mathbf{P}_{\text{interp}}^{\mathbf{T}}$; (2) $\mathbf{P}_{\text{interp}}\mathbf{S}_{\text{interp}}\mathbf{P}_{\text{interp}} = \mathbf{P}_{\text{interp}}$; and (3) $Tr[\mathbf{P}_{\text{interp}}\mathbf{S}_{\text{interp}}] = N_{\text{elec}}$, where N_{elec} is the number of electrons in the investigated system. Recently, the community[11,12,15–18] has realized that density matrices in the orthonormal basis are elements of a Grassmann manifold.[19,20] As a result, the mathematics of Grassmann manifolds can then be exploited to perform indirect interpolations on density matrices.

Our group has recently explored the utility of the Grassmann interpolation (G-Int) method to generate highly accurate $\mathbf{P}_{\text{interp}}$ for closed and unrestricted open-shell systems.[11,12] When $\mathbf{P}_{\text{interp}}$ is used as an SCF initial guess, its high quality leads to the extent that one can bypass performing SCF iterations and obtain *ab initio* energies directly. For instance in the case of ferrocene, the energies $E_{\text{initial}}^{\text{SCF}}$ obtained using $\mathbf{P}_{\text{interp}}$ directly only have an error of $\sim 10^{-6}$ E_{h} when compared with the results from fully converged SCF solutions.[11] In this work, we extended applications of G-Int in building spin contamination-free PESs using restricted open-shell methods. In addition, we will compare the accuracy of the DM-based G-Int method and the corresponding direct EB interpolation using the Lagrange interpolation.[21] Then, we will comment the effects of the Runge's phenomenon[12,22,23] on the DM-based and EB interpolation schemes. Lastly, the mitigation of the Runge's phenomenon by performing sampling on an unequally-spaced grid will be introduced and discussed.

2 Computational details

Fig. 1 briefly recapitulates the main concept of the G-Int method.[11,12,15] First, a collection of density matrices $\{\mathbf{P}_{\text{k}}\}$ at various geometries $\{r_{\text{k}}\}$ is sampled. Then, $\{\mathbf{P}_{\text{k}}\}$ is converted to $\{\overline{\mathbf{P}}_{\text{k}}\}$ in the orthonormal basis through $\overline{\mathbf{P}}_{\text{k}} = \mathbf{S}_{\text{k}}^{1/2}\mathbf{P}_{\text{k}}\mathbf{S}_{\text{k}}^{1/2}$. These $\{\overline{\mathbf{P}}_{\text{k}}\}$ are objects of the Grassmann manifold $\mathcal{M}_{\text{Gr}}$ and is depicted in Fig 1. A reference point $\mathbf{R}_0$ is then chosen on which the tangent plane $\mathcal{T}_{r_{\text{ref}}}\mathcal{M}_{\text{Gr}}$ will be defined. It has been shown that the interpolation accuracy is not sensitive with the choice for the reference point.[11]

Afterward, the $\{\overline{\mathbf{P}}_{\text{k}}\}$ is mapped to its corresponding set of vectors $\{\mathbf{\Gamma}_{\text{k}}\}$ in $\mathcal{T}_{r_{\text{ref}}}\mathcal{M}_{\text{Gr}}$. This is achieved through the use of Grassmann logarithm.[11,15,20] We note here that such mapping is of prime importance, because $\mathcal{M}_{\text{Gr}}$ is not a vector space, while $\mathcal{T}_{r_{\text{ref}}}\mathcal{M}_{\text{Gr}}$ is a vector space which possesses closure property. Meaning to say, a linear combination of $\{\mathbf{\Gamma}_{\text{k}}\}$ also belongs to $\mathcal{T}_{r_{\text{ref}}}\mathcal{M}_{\text{Gr}}$, as a result direct interpolations at $\mathcal{T}_{r_{\text{ref}}}\mathcal{M}_{\text{Gr}}$ can be performed to obtain $\mathbf{\Gamma}_{\text{unk}}$. In our current implementation, this interpolation is performed through the Lagrange interpolation method.[21] Finally, the density matrix at the desired geometry can be obtained by converting $\mathbf{\Gamma}_{\text{unk}}$ back to $\overline{\mathbf{P}}_{\text{unk}}$ by means of Grassmann exponential.[11,15,20] Afterward, $\overline{\mathbf{P}}_{\text{unk}}$ can be converted back to $\mathbf{P}_{\text{unk}}$, which can then be used as an initial guess in an SCF calculation or to predict the energy directly. For a more comprehensive description of the G-Int method, the reader is advised to read our previous works[11,12] as well as the work from Polack and co-workers.[15] All restricted open-shell calculations in this work were performed using a locally modified version of Q-Chem[24] interfaced with an external Python 3 code for G-Int which needs to be performed two times, one for $\mathbf{P}^{\alpha}$ and another for $\mathbf{P}^{\beta}$.

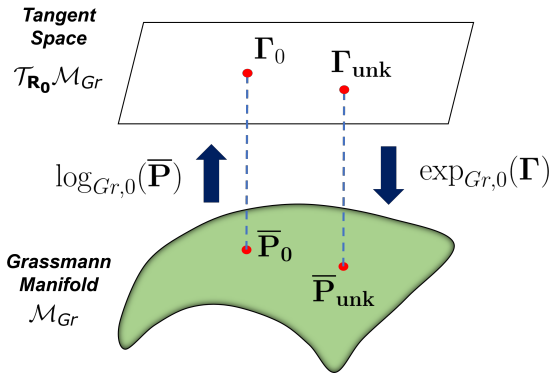

Fig. 1 Schematic representation of $\mathcal{M}_{\text{Gr}}$, $\mathcal{T}_{\mathbf{R_0}}\mathcal{M}_{\text{Gr}}$, and their mappings via Grassmann logarithm $\log_{\text{Gr},0}(\overline{\mathbf{P}})$ and Grassmann exponential $\exp_{\text{Gr},0}(\mathbf{\Gamma})$.

3 Results and discussion

We first demonstrate the newly developed restricted-open shell G-Int method for vanadium (II) oxide (VO) in its ground quartet state ($X^4\Sigma^-$) since transition metal oxide clusters were shown to suffer from significant spin contamination.[4,5] For VO, we choose the RO-revPBE0/def2-TZVP method to sample the density matrix along the V-O bond distance (r). Although HF or other DFT functionals can also be used to describe the electronic structure of VO, our purpose is to illustrate the use of G-Int to an open-shell system using a restricted open-shell method. The sampling was made in the 1.2 Å $\leq r \leq$ 2.0 Å range with dr = 0.10 Å as the step size. The sampled density matrices were then used to interpolate the density matrices along the 1.35 Å $\leq r \leq$ 1.75 Å range with dr = 0.10 Å using G-Int. The density matrix at r =1.2 Å was used as the reference point for defining $\mathcal{T}_{r_{\text{ref}}}\mathcal{M}_{\text{Gr}}$.

Table 1 summarizes the performance of G-Int for the interpolated points. We first compare how good the interpolated density matrices are with respect to the converged SCF results. This was done by calculating the Frobenius[25] norm $||\mathbf{\Delta P}^{\sigma}||_{\mathbf{F}}$ error for each

Table 1 Performance of G-Int in predicting the restricted open-shell (RO) density matrices of vanadium oxide for both α and β spins along the V-O bond distance (r) at the level of RO-revPBE0/def2-TZVP. The corresponding SCF energy and SCF error are also shown.

r(Å)	$\|\|\mathbf{\Delta P}^{\alpha}\|\|_{\mathbf{F}}$	$\|\|\mathbf{\Delta P}^{\beta}\|\|_{\mathbf{F}}$	$E^{\mathrm{SCF}}_{\mathrm{initial}}(E_{\mathrm{h}})$	$E^{\mathrm{SCF}}_{\mathrm{initial}} - E^{\mathrm{SCF}}_{\mathrm{conv}}(E_{\mathrm{h}})$
1.35	2.86×10^{-4}	2.16×10^{-4}	−1019.0549802263	1.30×10^{-8}
1.45	1.02×10^{-4}	6.66×10^{-5}	−1019.1093278846	2.20×10^{-9}
1.55	5.58×10^{-5}	3.15×10^{-5}	−1019.1286204093	8.00×10^{-10}
1.65	4.50×10^{-5}	2.72×10^{-5}	−1019.1261738812	4.00×10^{-10}
1.75	5.11×10^{-5}	3.58×10^{-5}	−1019.1114683897	8.00×10^{-10}

spin density matrix,

$$||\mathbf{\Delta P}^{\sigma}||_{\mathbf{F}} = \sqrt{\sum_{i,j} |(\mathbf{\Delta P}^{\sigma})_{ij}|^2}, \quad (1)$$

where $\mathbf{\Delta P}^{\sigma} = \mathbf{P}^{\sigma}_{\mathrm{interp}} - \mathbf{P}^{\sigma}_{\mathrm{conv}}$, which is the difference between the interpolated $\mathbf{P}^{\sigma}_{\mathrm{interp}}$ and converged $\mathbf{P}^{\sigma}_{\mathrm{conv}}$ density matrices. The superscript σ here denotes either an alpha or beta spin, $\sigma = \{\alpha, \beta\}$.

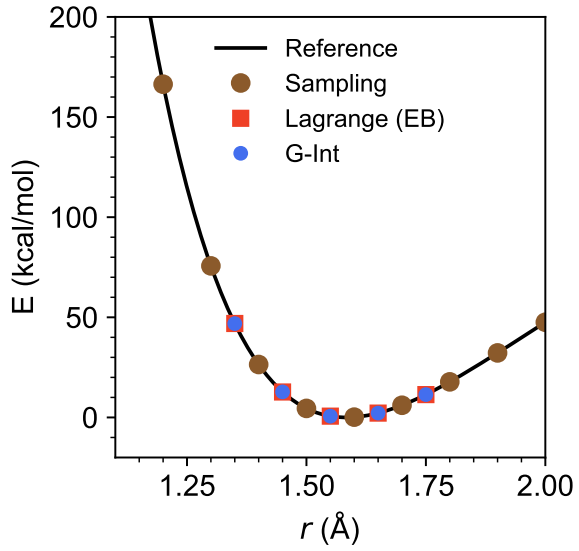

Fig. 2 RO-revPBE/def2-TZVP potential energy scan along the V-O bond distance (r) of vanadium oxide with reference scan (black), sampled data points used for interpolations (brown), energies obtained from the G-Int interpolated density matrices (blue), and directly interpolated energies using the energy-based (EB) Lagrange polynomial (red).

As shown in Table 1, $\mathbf{\Delta P}^{\alpha}$ and $\mathbf{\Delta P}^{\beta}$ have Frobenius norm errors between 2.72×10^{-5} to 2.86×10^{-4}. This implies that the interpolated density matrices are close to their converged counterparts. To better assess on how these Frobenius norm values translates to errors in the energy of the system, these $\mathbf{P}^{\sigma}_{\mathrm{interp}}$ are used to predict energies directly. Their corresponding energies $E^{\mathrm{SCF}}_{\mathrm{initial}}$ are then compared with the converged SCF energies $E^{\mathrm{SCF}}_{\mathrm{conv}}$. Table 1 shows $E^{\mathrm{SCF}}_{\mathrm{initial}}$ and $E^{\mathrm{SCF}}_{\mathrm{initial}} - E^{\mathrm{SCF}}_{\mathrm{conv}}$. The difference between $E^{\mathrm{SCF}}_{\mathrm{initial}}$ and $E^{\mathrm{SCF}}_{\mathrm{conv}}$ for the interpolated points is 1.30×10^{-8} E_{h} at most. These results implies that the $\mathbf{P}^{\sigma}_{\mathrm{interp}}$ are of superior quality to the extent that one can bypass the SCF iterations.

Fig. 2 shows a plot of a PES along the V-O coordinate of vanadium oxide. The reference curve (black) corresponds to a reference PES scan along the coordinate. The corresponding energies from the sampled density matrices are shown as brown dots in Fig. 2. The sampled density matrices were then used to generate the G-Int density matrices at the interpolated points, which are then used to evaluate the energies. Those energies are shown as blue dots in Fig. 2 and basically reproduce the reference curve, which indicates the good quality of these G-Int density matrices.

In the G-Int approach, the vectors on $\mathcal{T}_{r_{\mathrm{ref}}}\mathcal{M}_{\mathrm{Gr}}$ are interpolated using the Lagrange method. A natural question would be what is the performance of the direct EB Lagrange interpolation instead of doing the indirect DM-based G-Int. To address this question, we performed an EB Lagrange interpolation, and the results are shown as red squares in Fig. 2. Note that both the direct EB Lagrange interpolation and the indirect G-Int results agree well with the reference curve. Table 2 compares the performance of both methods with respect to the converged SCF energies $E^{\mathrm{SCF}}_{\mathrm{conv}}$ at several interpolated points. We note that between the two methods, the energies that were predicted by G-Int $(E_{\mathrm{G-Int}})$ are about four orders of magnitude more accurate than those obtained from the EB Lagrange interpolation $(E_{\mathrm{Lagrange(EB)}})$. The G-Int scheme, which automatically ensures the correct geometrical structure, properties, and physical requirements of the interpolated density matrix, generates a much more accurate PES as compared with the direct EB interpolation scheme. Furthermore, the interpolated density matrix can also be used to predict other molecular properties such as atomic charges.[12] Another interesting point is that $E_{\mathrm{G-Int}}$ in VO is always higher than the SCF solution and satisfies the variational principle which cannot be satisfied by the direct EB interpolation scheme.

Table 2 Comparison between the performance of the indirect G-Int and the energy-based (EB) Lagrange interpolations along the V-O bond distance (r) of vanadium oxide at the level of RO-revPBE/def2-TZVP.

r (Å)	$E_{\mathrm{G-Int}} - E^{\mathrm{SCF}}_{\mathrm{conv}}(E_{\mathrm{h}})$	$E_{\mathrm{Lagrange(EB)}} - E^{\mathrm{SCF}}_{\mathrm{conv}}(E_{\mathrm{h}})$
1.35	1.30×10^{-8}	1.03×10^{-4}
1.45	2.20×10^{-9}	-6.31×10^{-5}
1.55	8.00×10^{-10}	7.04×10^{-6}
1.65	4.00×10^{-10}	-2.01×10^{-5}
1.75	8.00×10^{-10}	-3.23×10^{-6}

To illustrate the use of G-Int in a larger system, we consider the rotation of the $-CH_2$ moiety in a benzyl radical which is a resonance-stabilized radical with high spin contamination in UHF.[26] Geometry optimization at the RO-B3LYP/def2-TZVP method reveals that its minimum structure is planar and belongs to the C_{2v} symmetry group. From the minimum structure, the density matrices were sampled in the $-90.00^{\circ} \leq \phi \leq 90.00^{\circ}$ range with $d\phi = 10.00^{\circ}$ as the step size. The information at $\phi = 0.00^{\circ}$ was used to define $\mathcal{T}_{\phi_{\mathrm{ref}}}\mathcal{M}_{\mathrm{Gr}}$. Interpolation was conducted in the

$-85.00^\circ \leq \phi \leq 85.00^\circ$ range with $d\phi = 10.00^\circ$ as the step size. Afterward, the SCF energies corresponding to the interpolated G-Int density matrices were evaluated. The Cartesian coordinate and atoms used in defining the dihedral angle ϕ can be found in Section A of the Supplementary Information (SI).

To assess the quality of the interpolated density matrices, let's consider the case at $\phi = 15.00^\circ$. The Frobenius norms are comparable for the interpolated α and β density matrices. In particular, $||\mathbf{\Delta P}^{\alpha}||_{\mathbf{F}} = 3.45 \times 10^{-4}$ and $||\mathbf{\Delta P}^{\beta}||_{\mathbf{F}} = 1.01 \times 10^{-4}$. The assessment for the rest of the interpolated points can be found in Section B of the SI. Fig 3 compares the performance of G-Int with other SCF initial guess schemes for the case of $\phi = 15.00^\circ$. The SCF calculation was performed using the geometric direct minimization (GDM) algorithm.[27] As shown in Fig. 3, G-Int outperforms all the other traditional SCF initial guess schemes with about 2, 5, and 7 times faster than SADMO, GWH, and CORE, respectively.

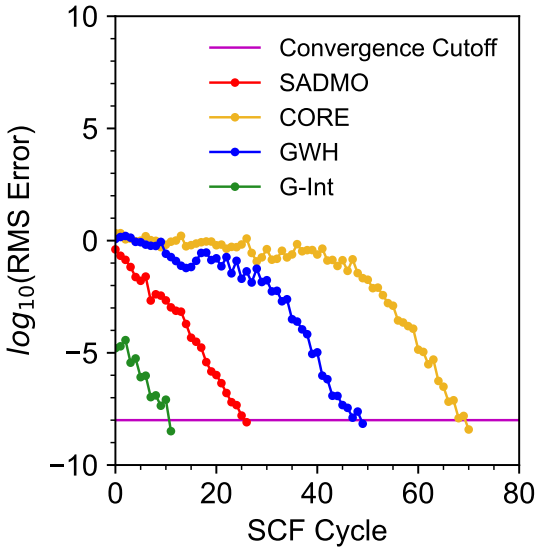

Fig. 3 Logarithm of the GDM algorithm's RMS error as a function of the SCF cycle number for a benzyl radical with $\phi = 15.00^\circ$ at the level of RO-B3LYP/def2-TZVP using several SCF initial guess schemes: CORE (golden rod) , GWH (blue), SADMO (red), and G-Int (green). The magenta line corresponds to $\log_{10}$ (1.00×10^{-8}), which is the SCF convergence criterion.

To compare qualitatively how good $E_{\mathrm{G-Int}}$ are with respect to their converged SCF energies, a rigid PES scan in the $-90.00^\circ \leq \phi \leq 90.00^\circ$ range was performed and is shown as a black curve in Fig. 4. Except for $\phi = \pm 85.00^\circ$ which are near the end of the interval, all of the interpolated points agrees fairly well with the reference curve. The small deviation between the reference and interpolated points at $\phi = \pm 85.00^\circ$ with an error up to 9.04×10^{-4} E_{h} is likely due to the Runge's phenomenon,[12,22,23] which is inherent to a Lagrange interpolation when an equally-spaced grid is used. The Runge's phenomenon is a problem of large oscillations which occurs at the edges of the interpolation interval and happens when a high-degree polynomial is used for the interpolation.

We then compare the performance of $E_{\mathrm{G-Int}}$ and $E_{\mathrm{Lagrange(EB)}}$ on the whole PES. As shown in Fig. 4, $E_{\mathrm{G-Int}}$ is one to four orders

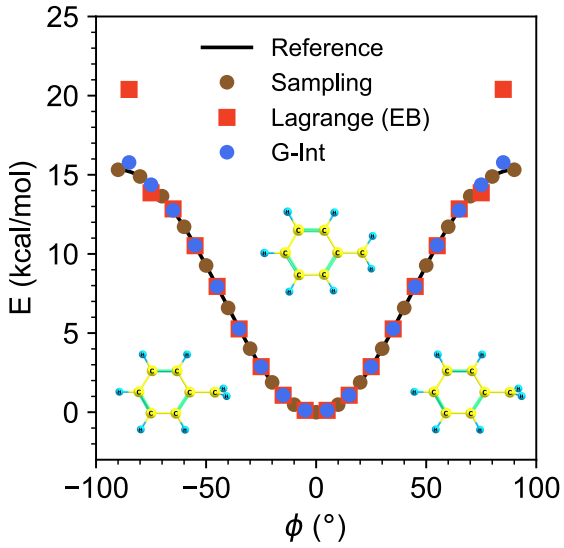

Fig. 4 RO-B3LYP/def2-TZVP rigid potential energy scan along the dihedral angle between the phenyl and $-CH_2$ moiety of a benzyl radical with reference scan (black), sampled data points used for interpolations (brown), energies obtained from the G-Int interpolated density matrices (blue), and directly interpolated energies using the energy-based (EB) Lagrange polynomial (red).

of magnitude more accurate than $E_{\mathrm{Lagrange(EB)}}$. In addition, $E_{\mathrm{G-Int}}$ still satisfies the variational principle, but $E_{\mathrm{Lagrange(EB)}}$ does not. $E_{\mathrm{Lagrange(EB)}}$ starts to have deviations at $\phi = \pm 75.00^\circ$ and show very large errors at $\phi = \pm 85.00^\circ$ as shown in Fig. 4. The energies at $\phi = \pm 85.00^\circ$ that were obtained from G-Int agrees way much better than those obtained from the direct EB Lagrange interpolation. Such finding suggests that the indirect Lagrange interpolation on $\mathcal{T}_{r_{\mathrm{ref}}}\mathcal{M}_{\mathrm{Gr}}$ (G-Int) appears to be less susceptible to the Runge's phenomenon, and therefore the indirect G-Int scheme outperforms the direct the EB Lagrange interpolation approach in mapping PESs. A more thorough study is needed to fully characterize this aspect which is currently explored in our group.

As mentioned earlier, the Runge's phenomenon associated with the G-Int method is an artifact of using an equally-spaced grid for the Lagrange interpolation.[12,22,23] To further investigate this phenomenon, we explore the case for methanesulfenyl chloride radical cation, $CH_3SCl^{\bullet+}$, serving as an illustrative and special example that further magnifies errors near the end of the interval attributed to Runge's phenomenon in flat PES regions. The ground doublet state geometry for $CH_3SCl^{\bullet+}$ was optimized at the level of revPBE0/def2-TZVP. Afterwards, a rigid potential scan along the H-C-S-Cl dihedral angle of this species was performed in the $-64.00^\circ \leq \phi \leq 64.00^\circ$ range with $d\phi = 8.00^\circ$. The density matrix at $\phi = 0.00^\circ$ was used in defining the tangent space. Fig. 5 shows that the potential curve is flat at both ends of the scan interval. A Lagrange-based G-Int for points on the flat regions would result to large errors when an equally-spaced grid is used since the Lagrange interpolating polynomial would tend to oscillate (Runge's phenomenon) near the end regions of the sampled grid.[22]

To investigate the severity of such errors, interpolation at se-

Table 3 Performance of G-Int in predicting the restricted open-shell (RO) density matrices using an unequally-spaced grid (a scaled Gauss-Chebyshev quadrature) for $CH_3SCl^{\bullet+}$ for both α and β spins along the H-C-S-Cl dihedral angle (ϕ) at the level of RO-revPBE0/def2-TZVP. The corresponding SCF energy and SCF error are also shown.

$\phi(^\circ)$	$\|\|\Delta\mathbf{P}^{\alpha}\|\|_{\mathbf{F}}$	$\|\|\Delta\mathbf{P}^{\beta}\|\|_{\mathbf{F}}$	$E^{\mathrm{SCF}}_{\mathrm{initial}}(E_{\mathrm{h}})$	$E^{\mathrm{SCF}}_{\mathrm{initial}} - E^{\mathrm{SCF}}_{\mathrm{conv}}(E_{\mathrm{h}})$
5.00	7.11×10^{-3}	6.95×10^{-3}	−897.8546774974	5.65×10^{-6}
10.00	4.07×10^{-3}	3.99×10^{-3}	−897.8547733728	1.86×10^{-6}
15.00	8.74×10^{-3}	8.56×10^{-3}	−897.8549082770	8.64×10^{-6}
31.00	5.86×10^{-2}	5.74×10^{-2}	−897.8552929056	3.92×10^{-4}
38.00	4.88×10^{-2}	4.79×10^{-2}	−897.8557856435	2.72×10^{-4}
45.00	1.20×10^{-2}	1.18×10^{-2}	−897.8563559055	1.64×10^{-5}
58.00	3.65×10^{-3}	3.59×10^{-3}	−897.8567110954	1.49×10^{-6}
60.00	7.77×10^{-3}	7.63×10^{-3}	−897.8567150402	6.74×10^{-6}
62.00	3.23×10^{-3}	3.17×10^{-3}	−897.8567205067	1.17×10^{-6}

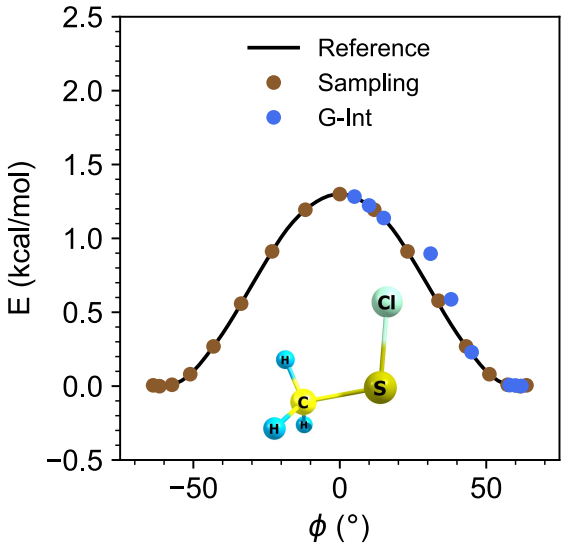

Fig. 5 RO-revPBE0/def2-TZVP potential energy scan along the H-C-S-Cl dihedral angle for methanesulfenyl chloride radical cation, $CH_3SCl^{\bullet+}$ with reference scan (black), sampled data points used for interpolations (brown), and energies obtained from the G-Int interpolated density matrices (blue) using the scaled Gauss-Chebyshev grid.

lected ϕ values near the end region were performed. Table S3 in Section C of the SI shows the performance of the interpolated points at the end region, $\phi = 58^\circ, 60^\circ,$ and 62°, using an equally-spaced grid. Notice that the Frobenius norm errors when the G-Int density matrices are compared with their converged SCF solutions are large. In particular, $||\Delta\mathbf{P}^{\alpha}||_{\mathbf{F}}$ is between 22.5 to 26.6, while $||\Delta\mathbf{P}^{\beta}||_{\mathbf{F}}$ is between 21.4 to 25.2. These large Frobenius norm errors, which is due to Runge's phenomenon, also produces large errors when the corresponding $E_{\mathrm{G-Int}}$ is compared with $E^{\mathrm{SCF}}_{\mathrm{conv}}$. As shown in Table S3, the $E_{\mathrm{G-Int}}$ deviate between 1.13 to 1.17 E_{h} for these three end points. Meanwhile, density matrices in the inner region of the sampling interval such as from $\phi = 5^\circ$ to $\phi = 45^\circ$ not only have low Frobenius norm errors for the alpha and beta density matrices, but also have a $E_{\mathrm{G-Int}}$ that agrees excellently with their $E^{\mathrm{SCF}}_{\mathrm{conv}}$ counterparts. As given in Table S3, the $E_{\mathrm{G-Int}} - E^{\mathrm{SCF}}_{\mathrm{conv}}$ for the representative points in the inner sampling region have an error of 2.46×10^{-7} E_{h} at most.

We now examine whether there is a correlation between the significant end-point errors in G-Int with respect to the "nearness" of the interpolated point from the reference point at which the tangent space $\mathcal{T}_{\phi_{\mathrm{ref}}}\mathcal{M}_{\mathrm{Gr}}$ is defined. Using the previously sampled points in the $-64.00^\circ \leq \phi \leq 64.00^\circ$ range with $d\phi = 8.00^\circ$ for $CH_3SCl^{\bullet+}$, we performed G-Int at $\phi = 58^\circ$ on tangent spaces defined at different reference points, $\phi_{\mathrm{ref}} \in \{0.00^\circ, 40.00^\circ, 64.00^\circ\}$. We found that the errors are not so sensitive with the choice for ϕ_{ref}. For example, when $\phi_{\mathrm{ref}} = 0.00^\circ$, the $E_{\mathrm{G-Int}} - E^{\mathrm{SCF}}_{\mathrm{conv}}$ is 1.17 E_{h}. Choosing a $\phi_{\mathrm{ref}} = 64.00^\circ$, which is much closer to the interpolated point only decreases the $E_{\mathrm{G-Int}} - E^{\mathrm{SCF}}_{\mathrm{conv}}$ to 1.13 E_{h} (Table S4 in Section D of the SI). Hence, these significant errors at the end-points do not stem from the choice of ϕ_{ref}. In essence, the current findings suggest that the origin of these substantial end-point errors is due to the well-known Runge's phenomenon,[22] inherent to the interpolation method (Lagrange method) when an equally-spaced grid is employed. It is noteworthy that significant end-point errors persist even when employing the direct energy-based Lagrange interpolation approach with an equally-spaced grid. In other words, these interpolation errors near the interval's ends are not specific to G-Int but rather stem from the well-known Runge's phenomenon in numerical analysis. Thus, changing the interpolation method is expected to alleviate the issue of undesired loss in accuracy attributed to Runge's phenomenon. A potential algorithm that alleviates the impact of Runge's phenomenon on an equally-spaced grid is the S-Runge algorithm, developed by De Marchi and co-workers.[28]

We note that it is also possible to mitigate the Runge's phenomenon by performing sampling on an unequally-spaced grid.[23] Table 3 shows the performance of G-Int when an unequal-space grid is used. This unequally-spaced grid was generated using a scaled Gauss-Chebyshev quadrature.[21] A total of seventeen points were generated in the range of -1 to 1. Afterwards, these generated points were then multiplied by 64°, which is the highest-end of the sampling interval. The resulting grid then was used to sample the density matrices along the H-C-S-Cl dihedral angle. Fig. 5 shows the sampled points in (brown), the reference scan potential (black), and a few representative interpolated points using the scaled Gauss-Chebyshev grid. Here we note that by using an unequally-spaced grid, the Runge's phenomenon can be largely mitigated as the interpolated points near the ends of the sampling interval have a much better accuracy this time with error up to 6.74×10^{-6} E_{h} for three points at the end region. Although the use of a scaled Gauss-Chebyshev quadra-

ture does introduce errors in the region between 30° and 40° where errors at $\phi = 31°$ and 38° increase to 3.92×10^{-4} E_h and 2.72×10^{-4} E_h, respectively, G-Int combined with points sampling on an unequally-spaced grid provides a much better PES than the one used with an equally-spaced grid. The errors introduced by an unequally-spaced grid in the middle range can be in principle reduced by sampling more points around that region. However, the oscillations due to the Runge's phenomenon introduced by an equally-spaced grid will be even larger if more sampling points are used. This works has demonstrated that the impact of Runge's phenomenon on Lagrange interpolation can be significantly reduced by utilizing an unequally-spaced grid. Consequently, an unequally-spaced grid sampling may be a more favorable choice for G-Int in constructing PESs for general applications. Our group is currently exploring various combinations of interpolating and sampling schemes to effectively overcome Runge's phenomenon.

4 Conclusions

In summary, we have demonstrated that the indirect G-Int scheme excels in accelerating the construction of spin contamination-free restricted open-shell PESs, surpassing the direct energy-based Lagrange interpolation approach in both vanadiun (II) oxide and benzyl radical. Additionally, in the special case of the methanesulfenyl chloride radical cation, characterized by a flat PES at the end region along the H-C-S-Cl dihedral angle, substantial oscillations occur due to the well-known Runge's phenomenon introduced by an equally-spaced grid. Our findings indicate that an unequally-spaced grid significantly mitigates the Runge's phenomenon, making it a suitable choice when combined with G-Int for constructing PESs, even for challenging systems. We anticipate that this work extends the applicability of G-Int to build PESs for open-shell systems without suffering from spin contamination. Our group is actively developing extensions of the G-Int method for larger systems and exploring alternative sampling schemes,with results to be presented in upcoming publications.

Conflicts of interest

There are no conflicts to declare.

Acknowledgements

This work was supported by start-up funds from the Virginia Commonwealth University College of Humanities and Sciences. This research used resources of the National Energy Research Scientific Computing Center, a DOE Office of Science User Facility supported by the Office of Science of the U.S. Department of Energy under Contract No. DE-AC02-05CH11231 using NERSC Award No. BES-ERCAP0020838. High Performance Computing resources provided by the High Performance Research Computing (HPRC) Core Facility at Virginia Commonwealth University (https://chipc.vcu.edu) were also used for conducting the research reported in this work.

Notes and references

1 A. I. Krylov, in *The Quantum Chemistry of Open-Shell Species*, John Wiley & Sons, Ltd, 2017, ch. 4, pp. 151–224.

2 A. Szabo and N. S. Ostlund, *Modern Quantum Chemistry : Introduction to Advanced Electronic Structure Theory*, Dover Publications, New York, 1982.

3 J. L. Sonnenberg, H. B. Schlegel and H. P. Hratchian, in *Spin Contamination in Inorganic Chemistry Calculations*, John Wiley & Sons, Ltd, 2011.

4 S. E. Waller, J. E. Mann, D. W. Rothgeb and C. C. Jarrold, *J. Phys. Chem. A*, 2012, **116**, 9639–9652.

5 L. M. Thompson and H. P. Hratchian, *J. Phys. Chem. A*, 2015, **119**, 8744–8751.

6 J. M. Wittbrodt and H. B. Schlegel, *J. Chem. Phys.*, 1996, **105**, 6574–6577.

7 J. H. Van Lenthe, R. Zwaans, H. J. J. Van Dam and M. F. Guest, *J. Comput. Chem.*, 2006, **27**, 926–932.

8 S. Lehtola, *J. Chem. Theory Comput.*, 2019, **15**, 1593–1604.

9 M. Wolfsberg and L. Helmholz, *J. Chem. Phys.*, 1952, **20**, 837–843.

10 F. Ballesteros and K. U. Lao, *J. Chem. Theory Comput.*, 2022, **18**, 179–191.

11 J. A. Tan and K. U. Lao, *J. Chem. Phys.*, 2023, **158**, 051101.

12 J. A. Tan and K. U. Lao, *J. Chem. Phys.*, 2023, **158**, 214104.

13 F. Ballesteros, J. A. Tan and K. U. Lao, *J. Chem. Phys.*, 2023, **159**, 074107.

14 H.-Y. Kwon, Z. Morrow, C. T. Kelley and E. Jakubikova, *J. Phys. Chem. A*, 2021, **125**, 9725–9735.

15 E. Polack, A. Mikhalev, G. Dusson, B. Stamm and F. Lipparini, *Mol. Phys.*, 2020, **118**, e1779834.

16 E. Polack, G. Dusson, B. Stamm and F. Lipparini, *J. Chem. Theory Comput.*, 2021, **17**, 6965–6973.

17 P. Mazzeo, S. Hashem, F. Lipparini, L. Cupellini and B. Mennucci, *J. Phys. Chem. Lett.*, 2023, **14**, 1222–1229.

18 F. Pes, E. Polack, P. Mazzeo, G. Dusson, B. Stamm and F. Lipparini, *J. Phys. Chem. Lett.*, 2023, **14**, 9720–9726.

19 L. W. Tu, *An introduction to manifolds*, Springer, New York, 2nd edn, 2011.

20 T. Bendokat, R. Zimmermann and P. A. Absil, *A Grassmann Manifold Handbook: Basic Geometry and Computational Aspects*, 2020, `https://arxiv.org/abs/2011.13699`.

21 J. F. Epperson, *An introduction to numerical methods and analysis*, John Wiley & Sons, Ltd., 2021.

22 L. Trefethen and J. Weideman, *J. Approx. Theory*, 1991, **65**, 247–260.

23 L. N. Trefethen, *Approximation Theory and Approximation Practice*, Society for Industrial and Applied Mathematics, Philadelphia, 2013.

24 E. Epifanovsky, A. T. B. Gilbert, X. Feng, J. Lee, Y. Mao, N. Mardirossian, P. Pokhilko, A. F. White, M. P. Coons, A. L. Dempwolff, Z. Gan, D. Hait, P. R. Horn, L. D. Jacobson, I. Kaliman, J. Kussmann, A. W. Lange, K. U. Lao, D. S. Levine, J. Liu, S. C. McKenzie, A. F. Morrison, K. D. Nanda, F. Plasser, D. R. Rehn, M. L. Vidal, Z.-Q. You, Y. Zhu, B. Alam, B. J. Albrecht, A. Aldossary, E. Alguire, J. H. Andersen, V. Athavale, D. Barton, K. Begam, A. Behn, N. Bellonzi, Y. A. Bernard, E. J. Berquist, H. G. A. Burton, A. Carreras, K. Carter-Fenk, R. Chakraborty, A. D. Chien, K. D. Closser, V. Cofer-Shabica,

S. Dasgupta, M. de Wergifosse, J. Deng, M. Diedenhofen, H. Do, S. Ehlert, P.-T. Fang, S. Fatehi, Q. Feng, T. Friedhoff, J. Gayvert, Q. Ge, G. Gidofalvi, M. Goldey, J. Gomes, C. E. González-Espinoza, S. Gulania, A. O. Gunina, M. W. D. Hanson-Heine, P. H. P. Harbach, A. Hauser, M. F. Herbst, M. Hernández Vera, M. Hodecker, Z. C. Holden, S. Houck, X. Huang, K. Hui, B. C. Huynh, M. Ivanov, Á. Jász, H. Ji, H. Jiang, B. Kaduk, S. Kähler, K. Khistyaev, J. Kim, G. Kis, P. Klunzinger, Z. Koczor-Benda, J. H. Koh, D. Kosenkov, L. Koulias, T. Kowalczyk, C. M. Krauter, K. Kue, A. Kunitsa, T. Kus, I. Ladjánszki, A. Landau, K. V. Lawler, D. Lefrancois, S. Lehtola, R. R. Li, Y.-P. Li, J. Liang, M. Liebenthal, H.-H. Lin, Y.-S. Lin, F. Liu, K.-Y. Liu, M. Loipersberger, A. Luenser, A. Manjanath, P. Manohar, E. Mansoor, S. F. Manzer, S.-P. Mao, A. V. Marenich, T. Markovich, S. Mason, S. A. Maurer, P. F. McLaughlin, M. F. S. J. Menger, J.-M. Mewes, S. A. Mewes, P. Morgante, J. W. Mullinax, K. J. Oosterbaan, G. Paran, A. C. Paul, S. K. Paul, F. Pavošević, Z. Pei, S. Prager, E. I. Proynov, Á. Rák, E. Ramos-Cordoba, B. Rana, A. E. Rask, A. Rettig, R. M. Richard, F. Rob, E. Rossomme, T. Scheele, M. Scheurer, M. Schneider, N. Sergueev, S. M. Sharada, W. Skomorowski, D. W. Small, C. J. Stein, Y.-C. Su, E. J. Sundstrom, Z. Tao, J. Thirman, G. J. Tornai, T. Tsuchimochi, N. M. Tubman, S. P. Veccham, O. Vydrov, J. Wenzel, J. Witte, A. Yamada, K. Yao, S. Yeganeh, S. R. Yost, A. Zech, I. Y. Zhang, X. Zhang, Y. Zhang, D. Zuev, A. Aspuru-Guzik, A. T. Bell, N. A. Besley, K. B. Bravaya, B. R. Brooks, D. Casanova, J.-D. Chai, S. Coriani, C. J. Cramer, G. Cserey, A. E. DePrince, R. A. DiStasio, A. Dreuw, B. D. Dunietz, T. R. Furlani, W. A. Goddard, S. Hammes-Schiffer, T. Head-Gordon, W. J. Hehre, C.-P. Hsu, T.-C. Jagau, Y. Jung, A. Klamt, J. Kong, D. S. Lambrecht, W. Liang, N. J. Mayhall, C. W. McCurdy, J. B. Neaton, C. Ochsenfeld, J. A. Parkhill, R. Peverati, V. A. Rassolov, Y. Shao, L. V. Slipchenko, T. Stauch, R. P. Steele, J. E. Subotnik, A. J. W. Thom, A. Tkatchenko, D. G. Truhlar, T. Van Voorhis, T. A. Wesolowski, K. B. Whaley, H. L. Woodcock, P. M. Zimmerman, S. Faraji, P. M. W. Gill, M. Head-Gordon, J. M. Herbert and A. I. Krylov, *J. Chem. Phys.*, 2021, **155**, 084801.

25 G. H. Golub, *Matrix computations*, Johns Hopkins University Press, Baltimore, Md, 2nd edn, 1989.

26 A. S. Menon and L. Radom, *J. Phys. Chem. A*, 2008, **112**, 13225–13230.

27 T. V. Voorhis and M. Head-Gordon, *Mol. Phys.*, 2002, **100**, 1713–1721.

28 S. De Marchi, F. Marchetti, E. Perracchione and D. Poggiali, *J. Comput. Appl. Math.*, 2020, **364**, 112347.